# 6

# CONCLUSION AND OUTLOOK

THE field of all–optical analog computing gained significant attention in the past and for quite some time seemed a promising alternative to standard electronic computing. However, as Moore's law kicked in, optical processors became quickly obsolete and were overwhelmed by what we nowadays mean by "computers".

The tremendous advances in nano–lithography that boosted the number of transistors per unit area also played a crucial role in the much more recent field of Nanophotonics. Metamaterials, metasurfaces, photonic crystals, plasmonics, and micro–resonators have now demonstrated the ability to mold the flow of light at the nano-scale with unprecedented precision. From this perspective, optical analog computing is still uncharted territory and the impact of nanophotonics on this field can be groundbreaking.

In this context, the work presented in this thesis helps to establish the field of all-optical processing via metasurfaces showing three different platforms that are compact and on-chip amenable. The possibility of integration into standard CMOS technology, in turn, enables exciting opportunities for hybrid analog-digital processing that operates at a higher data rate while simultaneously consuming less power.

Figure 6.1 shows an overview of the main experimental results presented in each chapter of the thesis.

In Chapter 2, we demonstrate how dielectric metasurfaces sustaining Fano resonances with suitably engineered dispersion can be designed to impart transfer functions in momentum space that correspond to $1^{st}$– and $2^{nd}$–order spatial differentiation. We show that the ideal amplitude and phase transfer functions can be realized over a relatively wide range of input angles spanning a numerical aperture up to 0.35 and a transmission amplitude larger than 0.8 can be achieved for large angles. Such NA ensures high spatial resolution and enables the implementation into standard imaging systems (e.g. smartphone cameras). Moreover, as our metasurface design operates in the image plane of the object and not in the Fourier plane, it can be placed directly onto the imaging chip for compact device implementations. The deviations from the ideal transfer functions, which are intrinsic to the design, are small enough to still achieve derivative operations close to ideal $1^{st}$- and $2^{nd}$-derivative. Furthermore, we experimentally demon-

strate metasurface-based optical processing using a suitably designed sub-wavelength array of Si nanobeams. As shown in Figure 6.1a, when the image of our institute logo is projected to the metasurface for resonant illumination ($\lambda$ = 726 nm), clear edge detection is achieved, as a result of the 2$^{nd}$-order spatial differentiation. Finally, we extend the metasurface for analog processing concept to 2D operations and unpolarized illumination. Optimized designs performing quasi-isotropic even- and odd-order spatial differentiation are presented and numerically demonstrate edge detection in all directions.

In Chapter 3, we couple a metasurface sustaining a Fano resonance to a gated $WS_2$ monolayer to achieve electrically-controllable optical processing. We leverage the impact of excitonic resonance quenching on the monolayer TMD's optical response to actively tune the metasurface transfer function. To demonstrate this, we design a device that acts as a high-pass filter that can be controlled by the presence (or absence) of excitons in the $WS_2$ monolayer. The optimum design achieves a numerical aperture of 0.2 and a transmission amplitude close to 0.8 at the maximum k-vector processed. Numerical tests on multiple input test functions and images clearly demonstrate reliable edge filtering that can be turned on and off at $\lambda$ = 626 nm and $\lambda$ = 620 nm. Next, we fabricate a chip containing several devices, each composed of an array of $TiO_x$ nanowires on a $WS_2$ monolayer gated via a MOSFET-like configuration (see Figure 6.1b). Optical reflectance spectra clearly show both the A-exciton feature and the GMR-based Fano lineshape. Figure 6.1b demonstrates reflectance modulation under an applied external bias, showing the potential of the proposed hybrid metasurface–2D-TMD platform.



To go beyond image processing tasks, in Chapter 4 we present a Si metasurface-based platform for analog computing that is able to solve Fredholm integral equations of the second kind using free-space visible radiation. Inverse design routines enable the implementation of a specific scattering matrix synthesizing a prescribed kernel into a Si metagrating. To prove the generality of this technique, we set as the optimization goal a random passive and reciprocal kernel. The optimum design provides a scattering matrix that is very close to the desired one at the target wavelength $\lambda$ = 706 nm. Next, a semi-transparent mirror is incorporated into the sample to provide adequate feedback and thus perform the required Neumann series solving the corresponding equation in the analog domain at the speed of light. The solution provided by the metasurface in simulation effectively solves the problem of interest and is very close to its ideal counterpart. The designed metagrating is patterned onto a Si-on-sapphire substrate (see Figure 6.1c) showing small deviations between experiment and simulations. The comparison between the retrieved experimental solution and the ideal solution with the chosen kernel shows good agreement at a slightly blue-shifted wavelength of $\lambda$ = 699 nm, as shown in Figure 6.1c. Visible wavelength operation enables a highly compact, ultra-thin device, which results into high processing speeds and the possibility of on-chip integration.

Finally, in Chapter 5 we apply the insights gained on grating design to a nanophotonic light trapping scheme in the near-IR wavelength range to boost the efficiency of high-performance GaInP/GaAs/Si triple-junction solar cells. We optimize a nanopatterned Ag back-reflector at the bottom of the Si sub-cell to redirect light at diffraction angles beyond the escape cone of the Si absorber. The back-reflector consists of a hexagonal array of silver nanodisks embedded in a PMMA layer and in direct contact with Si.

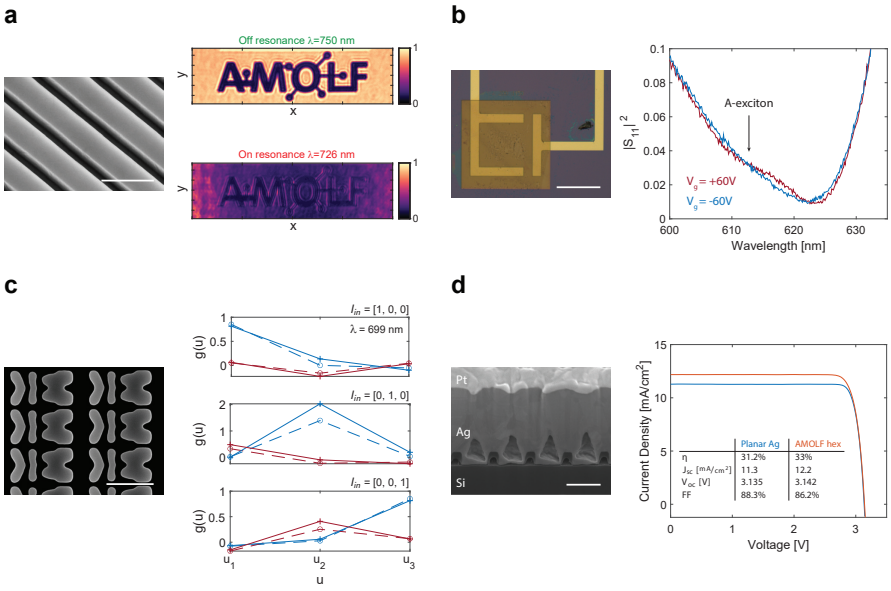


Figure 6.1: **a** Chapter 2. Left: tilted SEM image of the Si metasurface performing the 2nd–derivative operation (scalebar 400 nm). Right: optical microscopy image of the metasurface output for resonant ($\lambda$ = 726 nm) and off-resonant ($\lambda$ = 750 nm) illumination, demonstrating experimentally 2nd–order image differentiation. **b** Chapter 3. Left: optical microscopy image (scalebar 100 $\mu$m) of a representative completed device. Right: measured reflectance spectra for the same device as the bias voltage is switched from $V_g = +60$ V to $V_g = -60$ V. **c** Chapter 4. Left: top-view SEM image of the patterned Si metagrating (scalebar 500 nm). Right: estimated experimental analog solution (real and imaginary parts in blue and red respectively) of the integral equation (dashed line) compared to the ideal theoretical solution (solid lines), for the three orthogonal input vectors $(1,0,0)^\mathsf{T}$, $(0,1,0)^\mathsf{T}$, $(0,0,1)^\mathsf{T}$. The wavelength of operation in this simulation is $\lambda = 699$ nm. **d** Chapter 5. Left: SEM image of a FIB cross-section of the patterned Ag back-reflector on a triple–junction cell (scale bar 500 nm). Right: experimental one-sun I–V characteristics comparing the cell with the optimized hexagonal grating and its planar reference. Inset: performance parameters ($\eta$, $J_{sc}$, $V_{oc}$, and $FF$) of the same cell with planar and patterned back-reflector.

A simple interference model explains the physics governing reduced reflectance to the 0th diffraction order and further provides a guide on how to optimize the structural parameters. Next, the impact of the optimized design on the absorption in a thick Si slab is evaluated, highlighting an increase compared to a planar back–reflector as well as the design that is featured in the current record cell. Figure 6.1d shows a fabricated nanopatterned back-reflector on a full two–terminal triple–junction cell. The experimental external quantum efficiencies and one-sun current–voltage characteristics demonstrate a significant performance improvement over the planar reference (see inset of Figure 6.1d) without any measurable electrical degradation in the $V_{oc}$ due to the patterning process. These results highlight the potential to achieve efficiencies above the current record cell. Moreover, similar strategies can be applied to other Si-based tandem cells where standard random texture is not viable.

## OUTLOOK

The results of this thesis offer a path to a wide range of applications and can open new opportunities in hybrid optical and electronic computing that operates at low cost, low power, and small dimensions. Future research directions could include:

- Demonstration of other mathematical operations including convolutions with specific functions. Also, $1^{st}$–order spatial differentiation has still to be demonstrated experimentally. This, in turn, would require upgrades to the setup described in Section 2.6.2 targeting phase measurements in order to assess the asymmetric phase response of odd operations.

- Scaling–up of metasurface dimensions via SCIL and device integration. In order to apply the proposed designs to standard imaging chips, the patterned area has to be drastically increased to the cm-scale. This has been demonstrated to be possible without compromising resolution via SCIL, as shown in Chapter 5. It is worth stressing that the spatial differentiator metasurfaces presented in this thesis operate in the image plane and therefore can be directly applied onto the CCD of an existing imaging system (see Figure 6.2a). For best efficiency, the NA of the metasurface should match that of the imaging system. This is possible due to the design flexibility shown in Chapter 2.

- Monolithic compound optical elements. It is possible to envision a monolithic stack composed of a metalens, a free-space compressor metasurface, and a spatial differentiator, representing the ultimate miniaturization of an optical imaging system. Notice that precise lateral alignment of the components is not required.

- Non-reciprocal image processing. Optical isolators are components that allow light transmission only in one direction. This requires breaking reciprocity and can be achieved, among other schemes, relying on the optical Kerr effect: the permittivity of a material depends on the local electric field intensity via the third-order nonlinear susceptibility $\chi^{(3)}$. Fano resonators based on gratings supporting GMR and with Kerr nonlinearity have been proposed as isolators given their sharp response in frequency and transmission swinging from zero to a peak in a narrow bandwidth. If the resonator is designed to exhibit a different field distribution upon excitation from opposite directions, the Fano lineshape spectral location will also be dependent on the excitation port. This offset in wavelength between the Fano lineshape for forward and backward excitation defines a bandwidth where isolation can be achieved. As demonstrated in Chapter 2 the same structures can be designed to have a certain transfer function and thus to impart a given mathematical operation on an input signal. The combination of this concept with Kerr nonlinear isolators suggests the possibility of designing a structure with different transfer functions when excited from opposite directions. For instance, the minimum in transmission in the forward direction at normal incidence can be aligned to a maximum for backward propagation, leading in one case to edge detection (high-pass filter) yet to image blurring (low-pass filter) in the other direction, as schematically illustrated in Figure 6.2b.

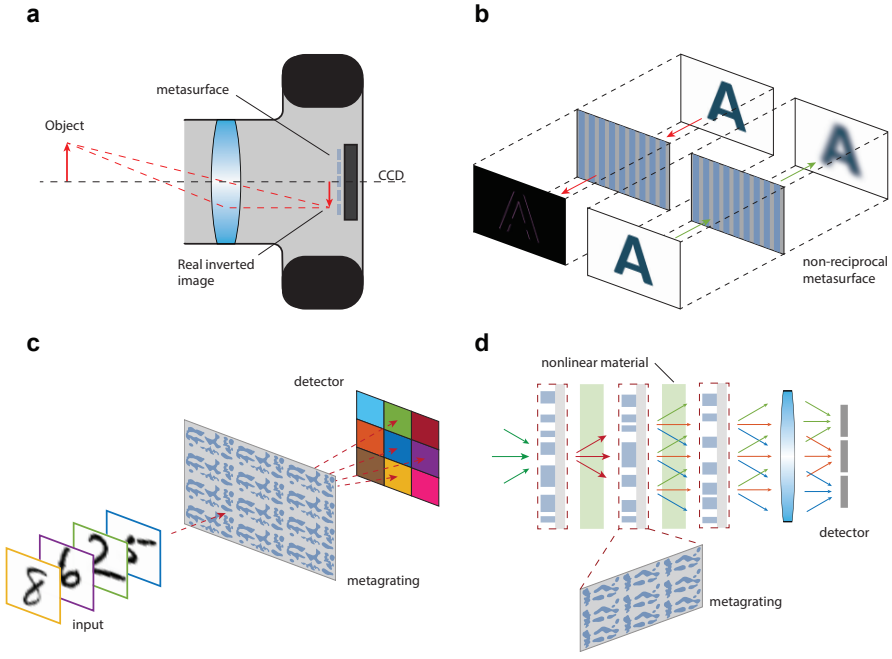


Figure 6.2: **a** Ray diagram for a standard imaging system. The metasurface can be placed directly on the imaging sensor (CCD). **b** Nonreciprocal image processing metasurface performing edge detection in the forward direction and image blurring in the backward direction. **c** A metagrating is designed to send light to a specific direction depending on the input character. **d** Schematic representation of a metagrating-based analog neural network. A wave signal is sent to the first layer and is diffracted by the first metasurface. Next, the power diffracted into the output channels is modulated by a nonlinear material (i.e. transmission changes with intensity). This process is repeated $N$ times (i.e. $N$ layers) until the final outcome is focused onto a standard detector.

Furthermore, a metasurface could be designed to have a transfer function that depends on the intensity of the input image.

- TMD-based metasurfaces with continuously tunable functionality. The excitonic resonance exploited in Chapter 3 shows a blue shift as the temperature goes down (see Figure 3.13). This can be used in combination with a metasurface sustaining a GMR to engineer the k-space response to continuously change as a function of temperature for a fixed illumination wavelength.

- Pattern recognition. Using inverse design routines, an optimized metagrating could be "trained" to recognize an input image by steering light to a specific diffraction channel (Figure 6.2c). This requires optimization of the k-space response of each element of the grating scattering matrix. Note that the unit cell can be large to allow for more degrees of freedom in the design and some diffraction channels may also be discarded. Essentially, this can be thought of as the character recognition

scheme based on matched filters illustrated in Chapter 1 but squeezed into a single surface.

- Metagrating-based analog neural networks. Neural networks can be thought of as a series of matrix multiplication and nonlinear renormalizations. Both ingredients are available and can be designed in the realm of nanophotonics.Utilizing topology optimization and adjoint method, we can devise and manufacture metasurfaces with designer scattering matrices. Regarding non-linearity, on the other end, there are several ways to obtain nonlinear behavior for light. For example with Kerr-type non-linearity, saturable absorber or coupling with atomic systems with discrete levels. The proposed device consists of a series of 2D crossed gratings with an inverse-designed unit cell that will provide the needed matrix multiplication (in phase and amplitude) between the diffraction channels in input and output. Next, a nonlinear material is sandwiched between the metasurfaces to provide the required renormalization. Eventually, a lens focuses the diffracted plane waves onto different pixels of a CCD detector. As schematically depicted in Figure 6.2d, a wave signal is sent to the first layer and is diffracted by the first metasurface. Next, the power diffracted into the output channels is modulated by a nonlinear material (i.e. transmission changes with intensity). This process is repeated $N$ times (i.e. $N$ layers) until the final outcome is focused onto a standard CCD detector. It is worth pointing out that, similar to standard neural networks, the connectivity of hidden layers can be increased at will by suitably changing the pitch of the metagratings and hence increasing the number of diffracted channels. One important advantage regarding fabrication is that lateral alignment across the layers is not needed. This in turn means that each metasurface can be fabricated independently.

- Nonlinear integral equation solver. By including nonlinear materials within the feedback system (e.g., replacing the $SiO_2$ spacer layer) of the integral solver proposed in Chapter 4, it would be possible to solve nonlinear mathematical problems. Additionally, nonlinearity could also be applied after processing the information via linear operations. Hence, a dedicated external nonlinear device could be designed to process the outputs of our metastructure.

To conclude, these and other opportunities will be explored in the near future at AMOLF (Amsterdam) in close collaboration with the groups of Prof. Andrea Alù at ASRC (New York) and Dr. Jorik van de Groep at Universiteit van Amsterdam.